The Astronomical Journal, 158:197 (15pp), 2019 November https://doi.org/10.3847/1538-3881/ab4136

KELT-24b: A $5M_J$ Planet on a 5.6 day Well-aligned Orbit around the Young $V = 8.3$ F-star HD 93148

Joseph E. Rodriguez[1,55], Jason D. Eastman[1], George Zhou[1,56], Samuel N. Quinn[1], Thomas G. Beatty[2], Kaloyan Penev[3], Marshall C. Johnson[4], Phillip A. Cargile[1], David W. Latham[1], Allyson Bieryla[1], Karen A. Collins[1], Courtney D. Dressing[5], David R. Ciardi[6], Howard M. Relles[1], Gabriel Murawski[7], Taku Nishiumi[8,9], Atsunori Yonehara[8], Ryo Ishimaru[10], Fumi Yoshida[10], Joao Gregorio[11], Michael B. Lund[6], Daniel J. Stevens[12,13], Keivan G. Stassun[14,15], B. Scott Gaudi[4], Knicole D. Colón[16], Joshua Pepper[17], Norio Narita[9,18,19,20], Supachai Awiphan[21], Pongpichit Chuanraksasat[21], Paul Benni[22], Roberto Zambelli[23], Lehman H. Garrison[1], Maurice L. Wilson[1], Matthew A. Cornachione[24,25], Sharon X. Wang[26], Jonathan Labadie-Bartz[27], Romy Rodríguez[4], Robert J. Siverd[14], Xinyu Yao[17], Daniel Bayliss[28,29], Perry Berlind[1], Michael L. Calkins[1], Jessie L. Christiansen[6], David H. Cohen[30], Dennis M. Conti[31], Ivan A. Curtis[32], D. L. Depoy[33,34], Gilbert A. Esquerdo[1], Phil Evans[35], Dax Feliz[14], Benjamin J. Fulton[6], Thomas W.-S. Holoien[36,57], David J. James[1,37], Tharindu Jayasinghe[4], Hannah Jang-Condell[38], Eric L. N. Jensen[30], John A. Johnson[1], Michael D. Joner[39], Somayeh Khakpash[17], John F. Kielkopf[40], Rudolf B. Kuhn[41,42], Mark Manner[43], Jennifer L. Marshall[33,34], Kim K. McLeod[44], Nate McCrady[45], Thomas E. Oberst[46], Ryan J. Oelkers[14], Matthew T. Penny[4], Phillip A. Reed[47], David H. Sliski[48], B. J. Shappee[49], Denise C. Stephens[39], Chris Stockdale[50], Thiam-Guan Tan[51], Mark Trueblood[52], Pat Trueblood[52], Steven Villanueva, Jr.[53,58], Robert A. Wittenmyer[54], and Jason T. Wright[12,13]

[1] Center for Astrophysics|Harvard & Smithsonian, 60 Garden Street, Cambridge, MA 02138, USA; joseph.rodriguez@cfa.harvard.edu
[2] Department of Astronomy and Steward Observatory, University of Arizona, Tucson, AZ 85721, USA
[3] Department of Physics, The University of Texas at Dallas, 800 West Campbell Road, Richardson, TX 75080-3021 USA
[4] Department of Astronomy, The Ohio State University, 140 West 18th Avenue, Columbus, OH 43210, USA
[5] Department of Astronomy, University of California Berkeley, Berkeley, CA 94720-3411, USA
[6] Caltech IPAC—NASA Exoplanet Science Institute 1200 E. California Avenue, Pasadena, CA 91125, USA
[7] Gabriel Murawski Private Observatory (SOTES), Poland
[8] Department of Physics, Faculty of Science, Kyoto Sangyo University, Kamigamo Motoyama, Kita-ku, Kyoto, 603-8555, Japan
[9] National Astronomical Observatory of Japan, 2-21-1 Osawa, Mitaka, Tokyo 181-8588, Japan
[10] Planetary Exploration Research Center, Chiba Institute of Technology, 2-17-1 Tsudanuma, Narashino, Chiba 275-0016, Japan
[11] Atalaia Group & CROW Observatory, Portalegre, Portugal
[12] Department of Astronomy & Astrophysics, The Pennsylvania State University, 525 Davey Lab, University Park, PA 16802, USA
[13] Center for Exoplanets and Habitable Worlds, The Pennsylvania State University, 525 Davey Lab, University Park, PA 16802, USA
[14] Department of Physics and Astronomy, Vanderbilt University, Nashville, TN 37235, USA
[15] Department of Physics, Fisk University, 1000 17th Avenue North, Nashville, TN 37208, USA
[16] Exoplanets and Stellar Astrophysics Laboratory, Code 667, NASA Goddard Space Flight Center, Greenbelt, MD 20771, USA
[17] Department of Physics, Lehigh University, 16 Memorial Drive East, Bethlehem, PA 18015, USA
[18] Astrobiology Center, 2-21-1 Osawa, Mitaka, Tokyo 181-8588, Japan
[19] JST, PRESTO, 2-21-1 Osawa, Mitaka, Tokyo 181-8588, Japan
[20] Instituto de Astrofísica de Canarias (IAC), E-38205 La Laguna, Tenerife, Spain
[21] National Astronomical Research Institute of Thailand, 260, Moo 4, T. Donkaew, A. Mae Rim, Chiang Mai, 50180, Thailand
[22] Acton Sky Portal (private observatory), Acton, MA 01720, USA
[23] Società Astronomica Lunae, Italy
[24] Department of Physics and Astronomy, University of Utah, 115 South 1400 East, Salt Lake City, UT 84112, USA
[25] Department of Physics, United States Naval Academy, 572C Holloway Road, Annapolis, MD 21402, USA
[26] Department of Terrestrial Magnetism, Carnegie Institution for Science, 5241 Broad Branch Road, NW, Washington, DC 20015, USA
[27] Instituto de Astronomia, Geofísica e Ciencias Atmosféricas, Universidade de São Paulo, Rua do Matão 1226, Cidade Universitãria, Sáo Paulo, SP 05508-900, Brazil
[28] Department of Physics, University of Warwick, Gibbet Hill Road, Coventry CV4 7AL, UK
[29] Centre for Exoplanets and Habitability, University of Warwick, Gibbet Hill Road, Coventry CV4 7AL, UK
[30] Department of Physics and Astronomy, Swarthmore College, Swarthmore, PA 19081, USA
[31] American Association of Variable Star Observers, 49 Bay State Road, Cambridge, MA 02138, USA
[32] Ivan Curtis Private Observatory, Australia
[33] George P. and Cynthia Woods Mitchell Institute for Fundamental Physics and Astronomy, Texas A&M University, College Station, TX77843 USA
[34] Department of Physics and Astronomy, Texas A&M university, College Station, TX 77843 USA
[35] El Sauce Observatory, Chile
[36] The Observatories of the Carnegie Institution for Science, 813 Santa Barbara Street, Pasadena, CA 91101, USA
[37] Black Hole Initiative at Harvard University, 20 Garden Street, Cambridge, MA 02138, USA
[38] Department of Physics & Astronomy, University of Wyoming, 1000 E University Avenue, Dept. 3905, Laramie, WY 82071, USA
[39] Department of Physics and Astronomy, Brigham Young University, Provo, UT 84602, USA
[40] Department of Physics and Astronomy, University of Louisville, Louisville, KY 40292, USA
[41] South African Astronomical Observatory, PO Box 9, Observatory, 7935, Cape Town, South Africa
[42] Southern African Large Telescope, PO Box 9, Observatory, 7935, Cape Town, South Africa
[43] Spot Observatory, Nashville, TN 37206, USA
[44] Department of Astronomy, Wellesley College, Wellesley, MA 02481, USA
[45] Department of Physics and Astronomy, University of Montana, 32 Campus Drive, No. 1080, Missoula, MT 59812 USA
[46] Department of Physics, Westminster College, New Wilmington, PA 16172, USA
[47] Department of Physical Sciences, Kutztown University, Kutztown, PA 19530, USA
[48] The University of Pennsylvania, Department of Physics and Astronomy, Philadelphia, PA, 19104, USA
[49] Institute for Astronomy, University of Hawai'i, 2680 Woodlawn Drive, Honolulu, HI 96822, USA

[50] Hazelwood Observatory, Churchill, Victoria, Australia
[51] Perth Exoplanet Survey Telescope, Australia
[52] Winer Observatory, PO Box 797, Sonoita, AZ 85637, USA
[53] Department of Physics and Kavli Institute for Astrophysics and Space Research, Massachusetts Institute of Technology, Cambridge, MA 02139, USA
[54] University of Southern Queensland, Centre for Astrophysics, West Street, Toowoomba, QLD 4350, Australia
Received 2019 June 7; revised 2019 August 9; accepted 2019 August 31; published 2019 October 23

Abstract

We present the discovery of KELT-24 b, a massive hot Jupiter orbiting a bright ($V = 8.3$ mag, $K = 7.2$ mag) young F-star with a period of 5.6 days. The host star, KELT-24 (HD 93148), has a $T_{\rm eff} = 6509^{+50}_{-49}$ K, a mass of $M_* = 1.460^{+0.055}_{-0.059}\,M_\odot$, a radius of $R_* = 1.506 \pm 0.022\,R_\odot$, and an age of $0.78^{+0.61}_{-0.42}$ Gyr. Its planetary companion (KELT-24 b) has a radius of $R_{\rm P} = 1.272 \pm 0.021\,R_{\rm J}$ and a mass of $M_{\rm P} = 5.18^{+0.21}_{-0.22}\,M_{\rm J}$, and from Doppler tomographic observations, we find that the planet's orbit is well-aligned to its host star's projected spin axis ($\lambda = 2.6^{+5.1}_{-3.6}$). The young age estimated for KELT-24 suggests that it only recently started to evolve from the zero-age main sequence. KELT-24 is the brightest star known to host a transiting giant planet with a period between 5 and 10 days. Although the circularization timescale is much longer than the age of the system, we do not detect a large eccentricity or significant misalignment that is expected from dynamical migration. The brightness of its host star and its moderate surface gravity make KELT-24b an intriguing target for detailed atmospheric characterization through spectroscopic emission measurements since it would bridge the current literature results that have primarily focused on lower mass hot Jupiters and a few brown dwarfs.

Unified Astronomy Thesaurus concepts: Transit photometry (1709); Exoplanet astronomy (486); Exoplanet detection methods (489); Radial velocity (1332)

Supporting material: data behind figure

1. Introduction

Despite confirmation of 4000 planets orbiting other stars, many of the questions raised by the first few discoveries over 20 years ago remain unanswered. One of the first possible planetary systems ever discovered was HD 114762 b, a massive Jupiter on an 84 day period around a late F-star (Latham et al. 1989). The inclination of the companion's orbit is not known, but it has a minimum mass of 11 $M_{\rm J}$ (Latham et al. 1989). Interestingly, over the past 30 years since this discovery, we now know of over 250 planets with a measured minimum mass between 4 and 13 Jupiter masses. Above $\sim$13 $M_{\rm J}$, a substellar companion can begin to fuse deuterium in its core, currently an arbitrary method for distinguishing planets and brown dwarfs. Another method to distinguish between brown dwarfs and giant planets is their formation mechanisms. Formation theories for brown dwarfs are similar to stars, in that they form either through gravitational instability or molecular cloud fragmentation while gas giant planet formation is likely dominated by core accretion (Chabrier et al. 2014, and references therein). However, there are inconsistencies between the deuterium burning and formation arguments to distinguish between planets and brown dwarfs since it is possible to form an object above the deuterium-burning limit through core accretion (Baraffe et al. 2008; Mollière & Mordasini 2012; Bodenheimer et al. 2013). The distinction between brown dwarfs and giant planets has been debated for decades (e.g., Chabrier 2003; Chabrier et al. 2007; Spiegel et al. 2011). The detailed characterization of massive Jupiters and low-mass brown dwarfs may shed light on their defining characteristics. However, the relatively low number of massive giant planets transiting bright host stars known, combined with their expected smaller atmospheric scale heights due to their higher surface gravity, has so far limited atmospheric studies of massive hot Jupiters and brown dwarfs.

The discovery of 51 Peg b (Mayor & Queloz 1995), a Jupiter-mass object orbiting a Sun-like star with a period of only 4.23 days, led to the idea that giant planets must undergo large-scale migration since it was commonly believed that giant planets could only form out past the ice line. However, it is not clear what mechanisms govern this migration, or if giant planets can form in situ close to the star (Batygin et al. 2016; Huang et al. 2016). One possibility is that giant planets migrate slowly and smoothly within the circumstellar gas-dust disk, resulting in well-aligned, nearly circular orbits (Goldreich & Tremaine 1980; Lin et al. 1996; D'Angelo et al. 2003). It is also thought that planetary migration may be heavily influenced by gravitational interactions with other bodies within the system. These interactions can result in highly eccentric and misaligned orbits (relative to the rotation axis of the star), that will dampen due to tidal effects, and is typically referred to as "high-eccentricity migration (HEM)" (Rasio & Ford 1996; Wu & Murray 2003; Fabrycky & Tremaine 2007; Nagasawa & Ida 2011; Wu & Lithwick 2011).

Due to their high rotation velocities ($v \sin I_* > 10$ km s^{-1}), hot (>6250 K) massive stars were avoided by many spectroscopic and photometric surveys for planets, including *Kepler* (Borucki et al. 2010). This was primarily due to the difficulty in measuring precise radial velocities (RVs) (<200 m s^{-1}) from rotationally broadened spectral lines. However, with the advancement of techniques to measure the Rossiter–McLaughlin effect (McLaughlin 1924; Rossiter 1924; Gaudi & Winn 2007; Cegla et al. 2016) and Doppler Tomography (Collier Cameron et al. 2010), a few dozen giant planets have now been confirmed around rapidly rotating F- and A-type stars. From these discoveries, a pattern has emerged where hot Jupiters around massive stars tend to be in misaligned orbits relative to their host star's rotation axis (Winn et al. 2010; Albrecht et al. 2012). This observed trend might be a signature that hot Jupiters predominantly migrate through HEM resulting in highly

[55] Future Faculty Leaders Fellow.
[56] NASA Hubble Fellow.
[57] Carnegie Fellow.
[58] Pappalardo Fellow.

eccentric and misaligned short-period orbits (see the review by Dawson & Johnson 2018 for a more in-depth discussion on tidal migration of hot Jupiters).

With the recent launch and early success of NASA's *Transiting Exoplanet Survey Satellite* (*TESS*) mission, we have now entered the next major chapter in the field of exoplanets. The primary mission for *TESS* is to discover and measure the masses of 50 small planets ($R < 4\ R_{\oplus}$) to understand their bulk compositions (Ricker et al. 2015). However, *TESS* will observe over 85% of the entire sky during its 2 year nominal mission, with the expectation of discovering thousands of giant planets (Barclay et al. 2018). There have already been over a dozen discoveries announced, including a number of giant planets on short-period, eccentric orbits (Brahm et al. 2019; Nielsen et al. 2019; Rodriguez et al. 2019). Also, unlike the ground-based surveys which struggle to discover longer period hot Jupiters due to their poor duty cycle, *TESS* should be complete for all short-period transiting hot Jupiters ($P \lesssim 5$ days). Short-duration ground-based surveys can be a great asset in the discovery of longer period giant planets ($P \gtrsim 5$ days) by precovering the ephemerides of the hundreds of single transits expected in the short baseline (∼27 days) of *TESS* observations (Villanueva et al. 2019; Yao et al. 2019). Additionally, detecting planets before their host stars are observed by *TESS* provides the opportunity to take advantage of the photometric precision and conduct detailed characterization of the planet's atmosphere through optical phase curves (see WASP-18b, Shporer et al. 2019).

In this paper, we present the discovery of KELT-24b, a massive ($5.18^{+0.21}_{-0.22}\ M_J$) Jupiter on a prograde orbit ($\lambda = 2.6^{+5.1}_{-3.6}$ degrees) orbiting a young ($0.78^{+0.61}_{-0.42}$ Gyr) F-star. The brightness of the host star ($V = 8.3$ mag) and the large planetary radius ($1.2\ R_J$) relative to its high mass, makes KELT-24 b well-suited for detailed characterization of its atmosphere. Additionally, KELT-24 b should be observed by *TESS* in the upcoming sectors 20 and 21, which should provide a great opportunity for simultaneous observations with the *Hubble Space Telescope* (*HST*).

The paper is organized in the following way. We describe our observations and the detection of KELT-24b as a candidate in Section 2. We present our global analysis of all observations in Section 3. In Section 4 we place the KELT-24 system in context with all known planets and given an overview of future detailed characterization observations for which it would be well-suited. We summarize our results and conclusions in Section 5.

2. Observations and Archival Data

2.1. KELT Photometry

The Kilodegree Extremely Little Telescope (KELT) survey[59] uses two 42 mm telescopes to discover hot Jupiters orbiting bright host stars ($7 < V < 12$), planets well-suited for detailed atmospheric characterization (Pepper et al. 2007, 2012, 2018). With one telescope in Sonita, AZ, and the other at the South African Astronomical Observatory (SAAO) in Sutherland, South Africa, KELT surveys over 85% of the entire sky with a 20–30 minute cadence. Each observing site has a Mamiya 645 80 mm $f/1.9$ 42 mm lens with a 4k × 4k Apogee CCD on a Paramount ME mount. This system provides a 26° × 26° field of view with a 23″ pixel scale. KELT has made a significant impact on our understanding of exoplanets around early-type stars, with the discovery of five transiting hot Jupiters orbiting A-stars (Zhou et al. 2016b; Gaudi et al. 2017; Lund et al. 2017; Johnson et al. 2018; Siverd et al. 2018) and six orbiting F-stars (Pepper et al. 2013; Collins et al. 2014; Bieryla et al. 2015; McLeod et al. 2017; Stevens et al. 2017; Temple et al. 2017).

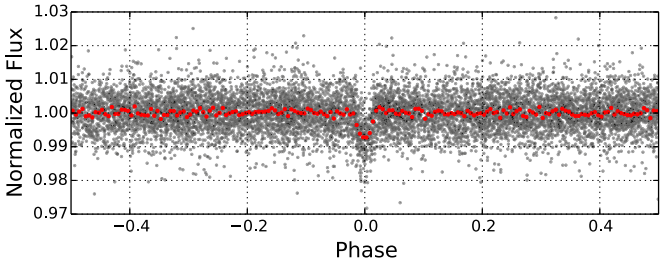

Figure 1. KELT discovery light curve of KELT-24 containing 10,181 observations from the KELT-North telescope phase-folded on the discovery period of 5.551477 days. The red points are the data binned on a 45 minute timescale.

The planetary companion orbiting HD 93148 (hereafter KELT-24 b) was identified from a joint analysis of five separate KELT-North fields that cover the celestial northern polar cap, KN25 through KN29 (although KELT-24 was only observed in two of the five fields). We reduced each of these KELT-North fields separately following the normal reduction process described in Siverd et al. (2012) and Kuhn et al. (2016). Once the raw light curves from each field were detrended, using the trend filtering algorithm (Kovács et al. 2005), we cross-matched each field to the Tycho-2 catalog (Høg et al. 2000). We then cross-matched the Tycho-2 IDs between the five polar cap fields from KELT-North and combined the detrended light curves into one per Tycho star. We then follow our normal candidate selection process on these combined light curves to identify a list of new polar cap candidates. We also examined the All-Sky Automated Survey for SuperNovae (ASAS-SN; Shappee et al. 2014; Kochanek et al. 2017; Jayasinghe et al. 2018) light curves of stars nearby the KELT transit candidates to exclude nearby eclipsing binaries. KELT-24 is located at J2000 $\alpha = 10^{\rm h}47^{\rm m}38\overset{\rm s}{.}35101$ $\delta = +71°39'21''.15672$ (Gaia Collaboration et al. 2018). KELT-24 was observed 10,181 times across the two KELT-North fields KN26 and KN27 from UT 2013 September 24 until UT 2017 December 31, after outliers were removed from our normal data reduction process. From our candidate selection process, we identified a candidate planet with a 5.551477 day period and a transit depth of 0.71%. See Figure 1 for the discovery light curve of KELT-24 b.

2.2. Ground-based Photometry from the KELT Follow-up Network

Unfortunately, systematic noise and astrophysical scenarios can mimic transit signals. To rule out nearby blended eclipsing binaries and precisely measure the depth, duration, and ephemeris, we obtained multiband photometric follow-up of KELT-24 b from the KELT Follow-Up Network (KELT-FUN, Collins et al. 2018). KELT-FUN is a worldwide network of amateur astronomers, small-college observatories, and observing time on the Las Cumbres Observatory telescope network (Brown et al. 2013). The telescopes range from 0.2 to 2 m in diameter, and this network has been responsible for the confirmation of dozens of giant planets, and the vetting of

[59] https://keltsurvey.org

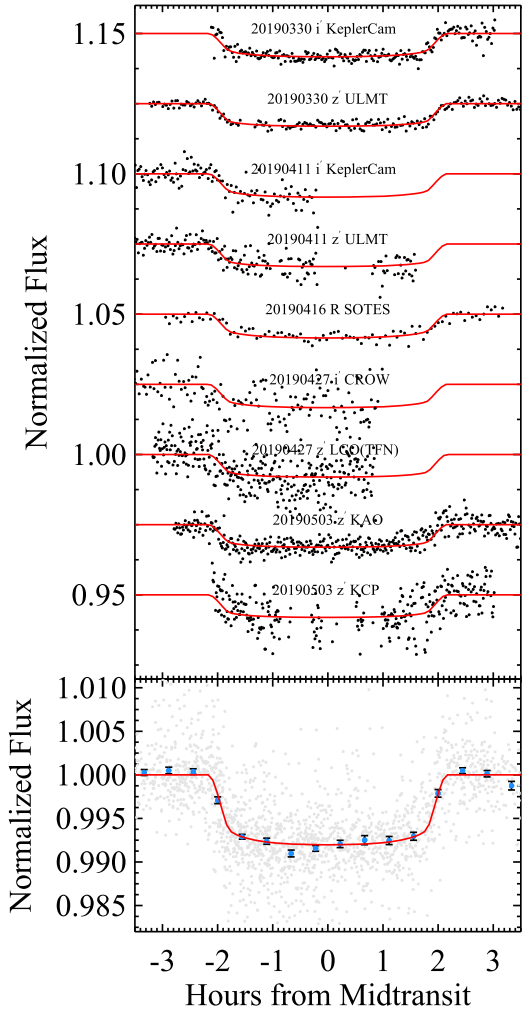

Figure 2. Top: the KELT-FUN light curves of KELT-24 b phased to global fit determined ephemeris shown in Table 5. See Table 2 for information on each KELT FUN observation. The relative flux points for each observation are shown in black and the EXOFASTv2 model is plotted in red. Bottom: all light curves combined and binned to 24 minutes (blue dots with black error bars). This combined light curve is not used in our analysis.

(The data used to create this figure are available.)

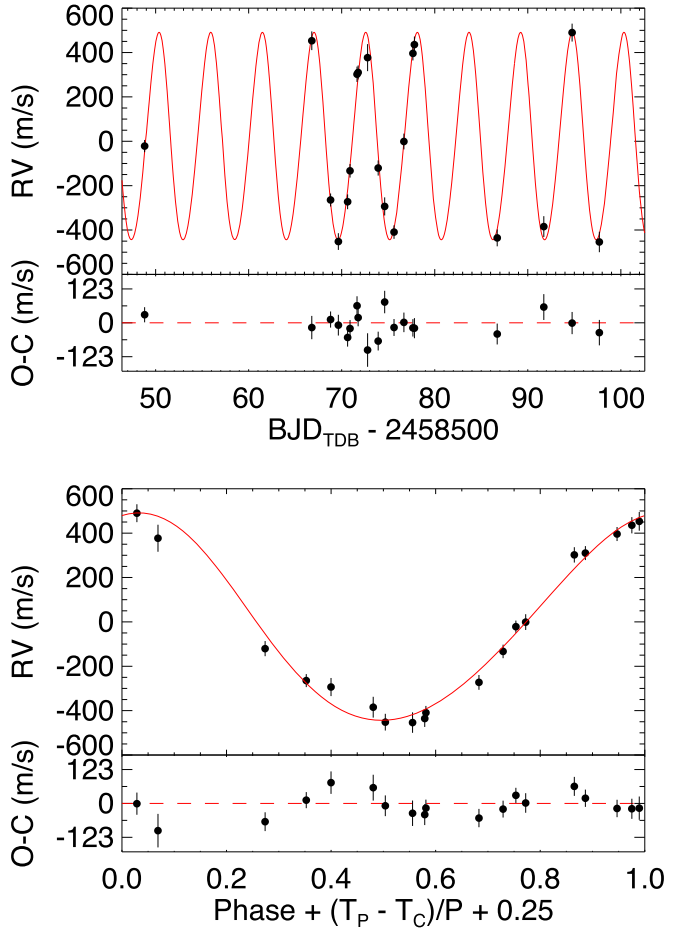

Figure 3. (Top) Radial velocity measurements from TRES (black). (Bottom) The radial velocity measurements are phase-folded to the best determined period by EXOFASTv2, 5.55 days. The EXOFASTv2 model is shown in red and the residuals to the best-fit are shown below each plot. We see no periodicity in the residuals from our fit.

thousands of candidates. We also observed a transit of KELT-24 b on UT 2019 May 3 from the Koyama Astronomical Observatory (KAO) located at Kyoto Sangyo University in Kyoto, Japan, and from the Kawabe Cosmic Park (KCP) observatory in Wakayama, Japan. We used the `TAPIR` software package (Jensen 2013) to schedule the observations of KELT-24. Most of the follow-up photometry was reduced and analyzed using the `AstroImageJ` astronomical observation analysis software (Collins et al. 2017). For information on the follow-up facilities that observed KELT-24b, see Table 2. The follow-up transits of KELT-24 b are shown in Figure 2.

2.3. TRES Spectroscopy

To confirm the planetary nature of KELT-24 b, we obtained 59 spectra using the Tillinghast Reflector Echelle Spectrograph (TRES; Fűrész 2008)[60] on the 1.5 m Tillinghast Reflector located at the Fred L. Whipple Observatory (FLWO) on Mt. Hopkins, AZ. TRES has a resolving power of $R \sim 44{,}000$, and has been highly successful in confirming exoplanet candidates from both ground- and space-based transit surveys. We reduced the TRES spectra and extracted RVs following the procedure described in Buchhave et al. (2010) and Quinn et al. (2012) with the exception of the creation of the template spectrum used. To create a high signal-to-noise ratio (S/N) template spectrum, we shifted and median-combined the out-of-transit spectra. We then used the median template to remove cosmic rays and replaced them with the appropriate section of the stellar spectrum rather than interpolating across the masked outliers. We cross-correlated the cleaned observed spectra against the median template to determine our final relative RVs (see Table 3 and Figure 3). We report RVs derived from only 19 of the 59 spectra in our orbital solution. Most of the excluded spectra were taken in-transit, for which the Rossiter–McLaughlin effect will systematically bias the RVs. We also reject all but one out-of-transit RV from the night of the transit observation, because inclusion of all of those RVs could bias the orbital solution. That is, in the presence of stellar activity on timescales longer than the sequence of out-of-transit spectra on that night, the formal uncertainty could end up being much smaller than the systematics induced by stellar activity. While including only one RV from that night does not eliminate the possibility that stellar activity can affect the orbital solution, it

[60] http://www.sao.arizona.edu/html/FLWO/60/TRES/GABORthesis.pdf

does prevent an outsized effect from a single epoch. We calculated bisector spans for the 19 TRES spectra contributing to the orbital solution following the method described in Torres et al. (2007). We see no significant correlation between the bisector spans and the RVs. We also see no large scatter above the RV uncertainties, which are small relative to the RV semi-amplitude.

To constrain the stellar parameters $T_{\rm eff}$ and [Fe/H] for our global analysis, we analyzed the TRES spectra using the Stellar Parameter Classification (SPC) package (Buchhave et al. 2012). We determined the effective temperature, metallicity, surface gravity, and rotational velocity of KELT-24 to be: $T_{\rm eff} = 6499 \pm 50$ K, $\log g_\star = 4.28 \pm 0.10$, and $[{\rm Fe/H}] = 0.16 \pm 0.08$. We measure $v \sin I_* = 19.46 \pm 0.18\,{\rm km\,s^{-1}}$ and a macroturbulent broadening of $10.47 \pm 1.47\,{\rm km\,s^{-1}}$ for KELT-24 following the method presented in Zhou et al. (2016a) and Zhou et al. (2018).

Of the 59 TRES spectra, 40 were taken during and immediately after the transit of KELT-24 b on UT 2019 March 31 with the aim of measuring the spectroscopic transit of the planet. The exposures during transit achieved an S/N of 70–90 per resolution element on the Mg b lines (5187 Å). During the transit, the planet successively blocks different parts of the rotating stellar disk, which is seen as an indentation on the spectroscopic line profile. By extracting this indentation from the stellar line profile of each spectrum, we can reveal the spectroscopic transit of the planet, a technique known as Doppler tomography (Collier Cameron et al. 2010). The Doppler tomographic (DT) signal of KELT-24 b was extracted from these spectra following the methodology from Zhou et al. (2016a). We fit the DT signal from TRES within our global fit (see Section 3 and Figure 4) to constrain the spin–orbit alignment of KELT-24 b.

To derive an absolute RV for KELT-24, we cross-correlated each TRES spectrum against the CfA library of synthetic spectra (see, e.g., Nordstroem et al. 1994; Latham et al. 2002), which employ Kurucz model atmospheres (Kurucz 1992). The instrumental zero-point is calculated using RV standard stars that are monitored nightly and placed on the absolute RV scale from Nidever et al. (2002). This results in an absolute velocity of the system barycenter of $-5.749 \pm 0.065\,{\rm km\,s^{-1}}$.

2.4. MINERVA Spectroscopy

We also obtained 37 1800 s spectroscopic exposures of KELT-24 using the MINiature Exoplanet Radial Velocity Array (MINERVA) during the entire night beginning UT 2019 March 31, of which 17 exposures were taken during the transit of KELT-24 b. MINERVA is an array of four PlaneWave CDK700 0.7 m telescopes located at Mt. Hopkins, Arizona (Swift et al. 2015; Wilson et al. 2019). The four telescopes simultaneously fiber feed an $R = 80{,}000$ KiwiSpec spectrograph (Barnes et al. 2012; Gibson et al. 2012), so each exposure contains a spectrum from the four telescopes, each covering roughly 500–630 nm. While MINERVA is typically calibrated with an iodine cell, we removed it during these exposures to increase throughput. Wilson et al. (2019) showed that the vacuum-stabilized, temperature-controlled spectrograph is stable on ∼year-long timescales, and so we did not expect significant variation of the spectrograph during the night. An approximate wavelength solution for the DT analysis was derived from archival thorium argon exposures.

Only two of the four telescopes showed a significant signal. This was the first attempt at guiding all night on the same target, and the star drifted off the fiber due to flexure between the fiber and the guide camera in the other two telescopes before the transit began, and so their data were not used in this analysis. The DT signal was extracted from the MINERVA in-transit spectra following the technique shown by Zhou et al. (2016a). We simultaneously fit the DT signal observed from each MINERVA telescope (see Section 3 and Figure 4 which shows the combined MINERVA DT signal for both telescopes).

2.5. Keck/NIRC2 AO Imaging

The follow-up photometric observations from KELT-FUN of KELT-24 can only detect bright nearby companions at a separation of a few arcseconds. Unfortunately, nearby unresolved companions can significantly influence the estimated planetary radius by diluting the transit depth (Ciardi et al. 2015). Therefore, to properly account for any photometric contamination from any unaccounted stellar sources, we observed KELT-24 with the Near Infrared Camera 2 (NIRC2) adaptive optics (AO) set up on the W. M. Keck Observatory on UT 2019 May 12 in the Br-γ band (see Figure 5). Since KELT-24 is very bright ($K = 7.154$), we chose the narrower Br-γ filter instead of the K-band. NIRC2 on KECK has a 1024×1024 CCD and $9.942\,{\rm mas\,pix^{-1}}$ pixel scale. Part of the detector (the lower left quadrant) suffers from higher than typical noise levels compared to the other quadrants. A three-point dither pattern was used to avoid this part of the detector. After sky removal and flat-fielding corrections were applied, the observations of KELT-24 were aligned and coadded to create the final image seen in Figure 5, and a final 5σ sensitivity curve as a function of spatial separation as shown embedded in the plot. We detected a nearby star in Br-γ with a contrast of 2.6 mag in the KECK NIRC2 AO images. *Gaia* detected the same star with a ΔG of 4.76 and a separation of $2\farcs064 \pm 0\farcs001$ (Gaia Collaboration et al. 2018). This star has a parallax of 11.108 ± 0.127 mas corresponding to a distance of 90.25 ± 1.03 pc, with a correction applied from Stassun & Torres (2018), and proper motions of $\mu_\alpha, \mu_\delta = -50.756 \pm 0.325, -37.811 \pm 0.200\,{\rm mas\,yr^{-1}}$. These proper motions are significantly different from the proper motions of KELT-24: $\mu_\alpha, \mu_\delta = -56.184 \pm 0.053, -34.808 \pm 0.064\,{\rm mas\,yr^{-1}}$. The difference in proper motion could be explained by the orbital motion of the nearby companion to KELT-24 but the estimated radial distances to each star from *Gaia* differ by 5.7 pc. Since the two stars only have a projected separation of $2\farcs064$ (186 au), they are physically separated by ∼5.7 pc. Therefore, it is not clear whether this companion is bound to KELT-24.

We determined the sensitivity to any additional nearby bound or unbound companions by injecting simulated sources with an S/N of 5 azimuthally around the primary target every 45° at separations of integer multiples of the central source's FWHM. The contrast limits at each injected location were determined from the brightness of the injected sources relative to KELT-24. We average all of the determined limits at each radial separation to establish the 5σ detection limit at that distance. The rms dispersion of these azimuthally averaged limits set the uncertainty at each radial separation (Furlan et al. 2017).

The nearby faint companion is blended in all of our photometric follow-up observations from KELT-FUN. To create the ∼0.7% transit seen in our follow-up photometry from KELT-FUN, this companion would need to have a ∼59%

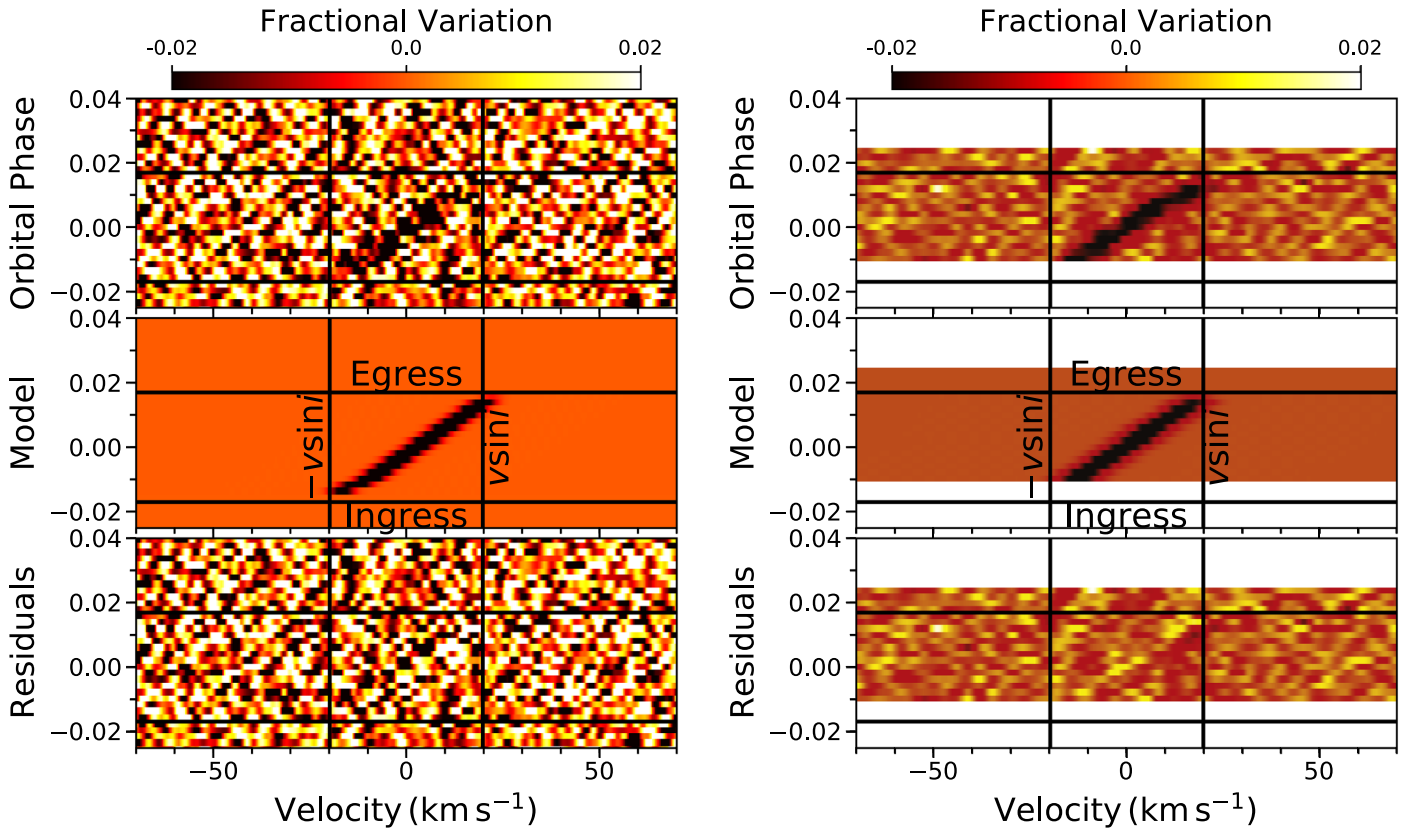

Figure 4. Doppler Tomographic transit of KELT-24 b on UT 2018 March 31 from (left) MINERVA and (right) TRES. The overall average of the line profiles from each instrument are plotted as a function of orbital phase and velocity. The MINERVA observation is the combined Doppler tomographic signal from telescopes 2 and 3 (see Section 2.4). The top panel in each plot represents the observed transit. The middle and bottom panels show the best-fit models and residuals after the model has been subtracted. MINERVA observed the entire transit, with baseline on each side, while TRES did not observe the beginning of the transit.

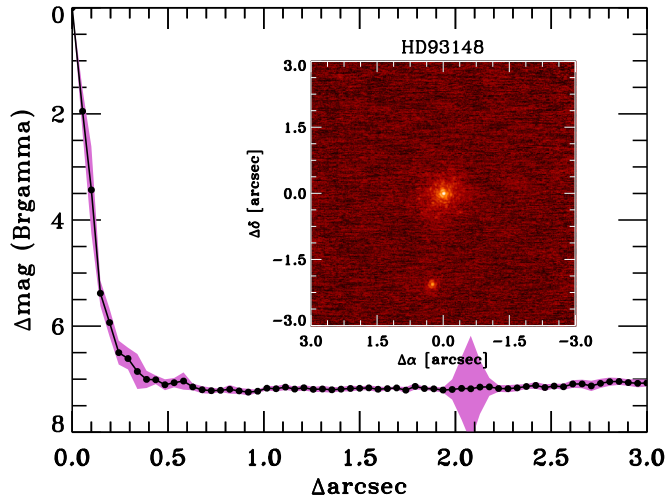

Figure 5. Brγ-band AO image from KECK NIRC2 and 5σ contrast curve for KELT-24. The purple swath represents the uncertainty on the 5σ contrast curve (see Section 2.5).

deep eclipse. While unlikely, it is not impossible for an eclipsing binary to have this deep of an eclipse. However, due to its small flux contribution to the spectroscopic line profiles, a companion this faint is not able to significantly influence the RVs. It is possible that a faint companion can slightly affect the measured RVs, but this would only be at the level of a few m s^{-1}, not the hundreds of m s^{-1} we detect for the orbit of KELT-24 b ($K = 458$ m s^{-1}, see the discussion of blended CCFs in Buchhave et al. 2011). Therefore, our subsequent RV follow up confirms that the planetary companion is orbiting our target star (KELT-24) and not the faint companion detected in *Gaia* and our KECK AO observations. To properly determine the size of KELT-24 b, we account for the companion's contribution in our global analysis (see Section 3).

2.6. SED Analysis

The spectral energy distribution (SED) was not included within our global fit due to the presence of the nearby companion seen by *Gaia* and our AO observations (see Section 2.5 and Figure 5). Therefore, we performed a two-component SED fit to determine the flux contribution from the companion in each of our follow-up photometric filters to use as an input into our global analysis (see Section 3). Using the available broadband photometry shown in Table 1, we fit the SED for KELT-24 from 0.2 to 20 μm (Figure 6). We applied a minimum uncertainty to the reported errors to account for a systematic error floor in the broadband magnitudes reported in the various catalogs. The nearby companion has a ΔG of 4.76 and a ΔBr-γ of 2.6 mag. We assumed both stars have the same extinction (A_V) and use the observed ΔG and ΔBr-γ to fit an SED for the faint companion (see Figure 6). The Kurucz (1992) stellar atmosphere models were used to fit each flux point for the primary and the NextGen model atmosphere grid were used for the companion (Hauschildt et al. 1999), and we use the SPC determined $T_{\rm eff}$ and [Fe/H] as Gaussian priors. We also used the $\log g_\star$ from the global fit (see Section 3) as a Gaussian prior. We allowed A_V to be a free parameter but constrain it to the

Table 1
Literature and Measured Properties for KELT-24

Other Identifiers			
	HD 93148		
	HIP 52796, TYC 4388-1652-1		
	BD+72 502, TIC 349827430		
Parameter	Description	Value	Source
α_{J2000}	Right ascension (R.A.)	10:47:38.35101	1
δ_{J2000}	Declination (Decl.)	+71:39:21.15672	1
l	Galactic longitude	135.°5728726	1
b	Galactic latitude	+42.°30147339	1
B_T	Tycho B_T mag	$8.913^{+0.020}_{-0.016}$	2
V_T	Tycho V_T mag	$8.389^{+0.020}_{-0.012}$	2
G	*Gaia G* mag	8.238 ± 0.02	1
J	2MASS J mag	7.408 ± 0.020	3
H	2MASS H mag	7.200 ± 0.04	3
K_S	2MASS K_S mag	7.154 ± 0.02	3
WISE1	*WISE1* mag	7.106 ± 0.039	4
WISE2	*WISE2* mag	$7.134^{+0.030}_{-0.019}$	4
WISE3	*WISE3* mag	$7.148^{+0.030}_{-0.017}$	4
WISE4	*WISE4* mag	$7.184^{+0.1}_{-0.098}$	4
μ_α	*Gaia* DR2 proper motion in R.A. (mas yr^{-1})	−56.184 ± 0.053	1
μ_δ	*Gaia* DR2 proper motion in decl. (mas yr^{-1})	−34.808 ± 0.064	1
π[a]	*Gaia* Parallax (mas)	10.414 ± 0.0469[a]	1
RV	Systemic radial velocity (km s^{-1})	−5.749 ± 0.065	Section 2.3
d	Distance (pc)	96.025 ± 0.306[a]	1
U[b]	Space velocity (km s^{-1})	−11.00 ± 0.11	Section 2.7
V	Space velocity (km s^{-1})	−9.36 ± 0.10	Section 2.7
W	Space velocity (km s^{-1})	0.11 ± 0.05	Section 2.7

Notes. The uncertainties of the photometry have a systematic error floor applied.
[a] Values have been corrected for the −0.82 μas offset as reported by Stassun & Torres (2018).
[b] U is in the direction of the Galactic center.
References. (1) Gaia Collaboration et al. (2018); (2) Høg et al. (2000); (3) Cutri et al. (2003); (4) Zacharias et al. (2017).

maximum permitted line-of-sight extinction from Schlegel et al. (1998).

The final SED fit has a reduced χ^2 of 2.7, an extinction of $A_V = 0.11 \pm 0.02$ mag (see Figure 6), and an unextincted bolometric flux received at Earth of $F_{\rm bol} = 1.309 \pm 0.015 \times 10^{-10}$ erg s^{-1} cm^{-2} (correcting for the contamination of the companion). We combined the bolometric flux with the $T_{\rm eff}$ from our SPC analysis (which was adopted for this fit) to measure the radius of KELT-24 to be $R_\star = 1.526 \pm 0.022\,R_\odot$. We enforced a Gaussian prior on R_* in our global fit (see Section 3). The flux contribution from the nearby companion is 1.01% (R), 1.79% (i'), and 2.73% (z').

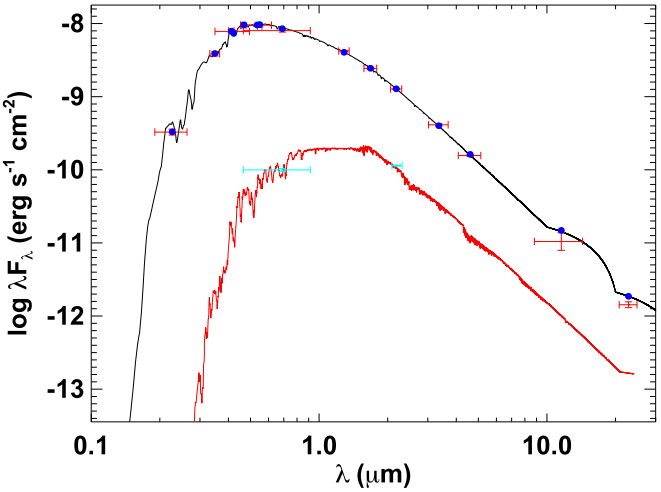

Figure 6. Two-component SED fit for KELT-24 and its companion. The blue points are the predicted integrated fluxes and the red points are the observed values at the corresponding passbands. The width of the bandpasses are the horizontal red error bars and the vertical errors represent the 1σ uncertainties. The cyan points are the G and Br-γ fluxes from *Gaia* and our AO observations (see Section 2.5). The best-fit atmospheric model for KELT-24 is shown by the black solid line and the companion is in red.

2.7. Location in the Galaxy, UVW Space Motion, and Galactic Population

We determined the three-dimensional (3D) Galactic space motion of KELT-24 to understand its location within the Milky Way galaxy and the Galactic population it belongs to. KELT-24 is located at $\alpha_{J2000} = 10^{\rm h}47^{\rm m}38\overset{\rm s}{.}351$ and $\delta_{J2000} = +71°39'21\overset{''}{.}157$, and from *Gaia* DR2 the parallax is 10.414 ± 0.0469 mas (after applying the correction from Stassun & Torres 2018). Ignoring the Lutz–Kelker bias, which should be negligible (Lutz & Kelker 1973), this star is located at a distance of 96.02 ± 0.43 pc from the Sun. Combining the sky position and distance, KELT-24 is located at a vertical (Z–$Z_\odot$) distance of 64.6 pc from the Sun. Bovy (2017) estimates from *Gaia* that the Sun is located at a vertical distance above the plane of $Z_\odot \sim 30$ pc. Therefore, KELT-24 is located at $Z \sim 100$ pc above the plane. This is the typical scale height for mid-to-late F thin disk stars (Bovy 2017). Using the *Gaia* parallax and proper motions (μ_α, μ_δ) = (−56.184 ± 0.053, −34.808 ± 0.064 mas yr^{-1}) and the absolute RV as determined from the TRES spectroscopy of −5.749 ± 0.065 km s^{-1}, we calculated the 3D Galactic space motion of (U, V, W) = (−11.00 ± 0.11, −9.36 ± 0.10, 0.11 ± 0.05) km s^{-1}, where positive U is in the direction of the Galactic center and adopting the Coşkunoğlu et al. (2011) determination of the solar motion with respect to the local standard of rest. The relatively low W velocity of KELT-24 suggests that KELT 24 may be close to its maximum excursion above the plane. KELT-24 has a 99.5% chance of being located in the thin disk, according to the classification of Bensby et al. (2003). The location of KELT-24 and its relatively low UVW velocities are both consistent with it being a young star, which corroborates the relatively young age inferred from evolutionary models (see Figure 7). The only association that is close to the estimated distance (96 pc) and UVW velocities of KELT-24 is the extended Ursa Major moving group. While the distance and 3D space motion of KELT-24 are clearly inconsistent with the core of the association (~24 pc), its distance is consistent with known members of the Ursa Major moving group stream (~100 pc).

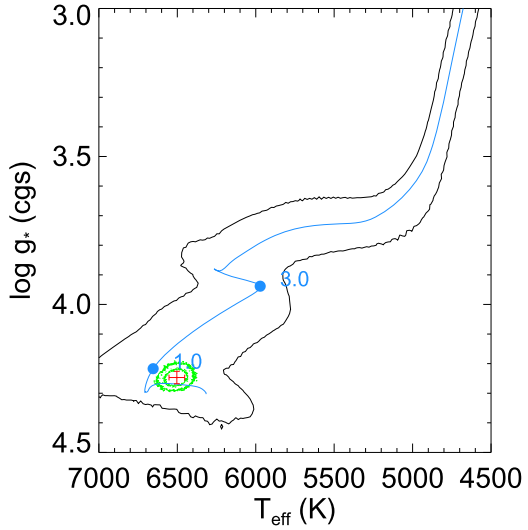

Figure 7. Best-fitting MIST track is shown by the blue line. The 3σ contours for the MIST evolutionary tracks are shown in black. The median values and 1σ errors from our global fit for $T_{\rm eff}$ and [Fe/H] are shown in red with the corresponding 3σ contours in green. The blue points represent the 1.0 and 3.0 Gyr positions along the MIST track.

However, a full UVW analysis of the entire association using the *Gaia* DR2 proper motions and distances are needed to conclusively determine whether KELT-24 is a member of the Ursa Major association. A detailed analysis of whether or not KELT-24 is a member of the Ursa Major association is well outside the scope of this paper, but we advocate that this is a worthwhile exercise, particularly given the other evidence for the youth of the host star presented in this paper.

3. EXOFASTv2 Global Fit for KELT-24

To understand the system parameters and place KELT-24 b in the context of all known planets, we globally fit all available photometry and spectroscopic observations using the publicly available exoplanet modeling suite EXOFASTv2 (Eastman et al. 2013; Eastman 2017; Eastman et al. 2019). We simultaneously fit the transit light curves from KELT-FUN (see Table 2 and Figure 2) with the RVs from TRES (see Table 3 and Figure 3). We enforced a Gaussian prior on the ephemeris of $T_C = 2457147.0522 \pm 0.0021$ $\rm BJD_{TDB}$ and $P = 5.551467 \pm 0.000034$ days from an EXOFASTv2 fit of just the KELT-North data. Within this analysis we also fit the DT signals observed on UT 2019 March 31 by MINERVA (two telescopes fit separately) and TRES (see Figure 4). The host star was characterized within the fit using the MESA Isochrones and Stellar Tracks (MIST) stellar evolution models (Paxton et al. 2011, 2013, 2015; Dotter 2016; Choi et al. 2016). The best-fit MIST evolutionary track is shown in Figure 7. From the SPC analysis of the TRES spectra (see Section 2.3), we enforced a Gaussian prior on $T_{\rm eff}$ (6499 ± 50 K), [Fe/H] (0.16 ± 0.08), and $v \sin I_*$ (19.458 ± 0.182 km s^{-1}). From *Gaia*, AO, and our two-component SED fit, we know that the nearby companion contributes 1.01% in R, 1.79% in i', and 2.73% in z'. To properly account for this contribution in the follow-up observations, we used these flux contributions with a 5% error as Gaussian priors in the EXOFASTv2 global fit. We note that the dilution prior on the follow-up photometry has no influence on the determined results. We also placed a prior on the radius of KELT-24 of $R_\star = 1.526 \pm 0.022\,R_\odot$, from our two-component SED fit. The final results from our EXOFASTv2 fit of the KELT-24 system are shown in Tables 4–6. We refer the reader to Table 3 in Eastman et al. (2019) for a list of the derived and fitted parameters in EXOFASTv2.

The KELT-North data has a time baseline of over 4 years, covering 64 different transits of KELT-24 b. Therefore, we explored the possibility of including the KELT-North photometry in the EXOFASTv2 fit to provide a better constraint on the ephemeris of the transit for future follow-up. However, we ran tests to ensure that the lower precision of the KELT-North photometry did not significantly influence the resulting system parameters. As a result of KELT-24 being observed in two separate fields and KELT avoiding observing within 50° of the moon, the number of observations in each transit varies significantly, with a maximum of 54 observations over a 4.9 hr transit (plus $\sim$ 1 hr baseline on each side). We ran two separate EXOFASTv2 fits, one as described in the previous paragraph that excluded the KELT-North data but placed a Gaussian prior on the ephemeris of KELT-24 b (T_C and period) from an EXOFASTv2 fit of just the KELT-North data. We also ran another fit where we included all 64 transits from KELT-North plus the KELT-FUN follow-up transits (see Figure 2). From this test, we saw no evidence that the inclusion of the KELT-North observations significantly influenced the results since the two fits were consistent to within $<1\sigma$ on all parameters. We did see a small (17.5%) improvement on the precision of KELT-24 b's period when including the KELT-North transits in the global fit. We note that this difference in precision corresponds to <1 s. The optimal time of conjunction had a similar precision between the two fits. We did notice that the inclusion of the KELT data resulted in a duration that is shorter (than the fit excluding the KELT data) by 25 s. Although this is within the 1σ uncertainty on the transit duration from our results (see Table 5), we choose to not include the KELT observations within the global fit as a precaution.

4. Discussion

KELT-24 b has some key characteristics that make it a compelling target for detailed characterization. Specifically, the host star is very bright, $V = 8.3$ mag, and the planet is quite massive, $5.18^{+0.21}_{-0.22}\,M_{\rm J}$. With such a high mass, it is interesting to see some signs that it is inflated ($R_{\rm P} = 1.272 \pm 0.021$ $R_{\rm J}$). However, this is not unique to this system since many massive hot Jupiters have inflated radii. Of all the hot Jupiters known, KELT-24 b is one of only a few dozen massive ($M_{\rm P} = 4$–13 $M_{\rm J}$) hot Jupiters ($P < 10$ days) with a host star bright enough ($V < 13$ mag) to permit detailed characterization.[61] At $V = 8.3$ mag, KELT-24 is the brightest known planetary host in this regime (see Figure 8). The host star, KELT-24, has a mass of $M_\star = 1.460^{+0.055}_{-0.059}\,M_\odot$, a radius of $R_\star = 1.506 \pm 0.022\,R_\odot$, and an age of $0.78^{+0.61}_{-0.42}$ Gyr. It is the brightest star known to host a transiting giant planet with a period between 5 and 10 days, and one of the longest period planets discovered from ground-based surveys. Interestingly, HAT-P-2b (Bakos et al. 2007) is quite similar to KELT-24 b in that they have almost the same orbital period (5.63 days compared to 5.55 days), similar planetary masses (9.0 $M_{\rm J}$ compared to 5.2 $M_{\rm J}$), and both host stars that are very bright (HAT-P-2 is $V = 8.7$ mag). The relatively

[61] https://exoplanetarchive.ipac.caltech.edu/; Akeson et al. (2013); UT 2019 May 07.

Table 2
Photometric Follow-up Observations of KELT-24 b and the Detrending Parameters Used for the Global Fit

Observatory	Date (UT)	Diameter (m)	Filter	FOV	Pixel Scale	Exposure (s)	Detrending
ULMT	2019 Mar 30	0.6096	z'	$26\farcm8 \times 26\farcm8$	$0\farcs39$	100	airmass, x coordinates
FLWO/KeplerCam	2019 Mar 30	1.2	i'	$23\farcm1 \times 23\farcm1$	$0\farcs37$	60	airmass
ULMT	2019 Apr 11	0.6096	z'	$26\farcm8 \times 26\farcm8$	$0\farcs39$	100	None
FLWO/KeplerCam	2019 Apr 11	1.2	i'	$23\farcm1 \times 23\farcm1$	$0\farcs37$	90	airmass
SOTES	2019 Apr 16	0.08	R	$84' \times 57'$	$1\farcs52$	240	airmass
CROW	2019 Apr 27	0.354	i'	$23' \times 18'$	$0\farcs66$	60	airmass
LCO TFN	2019 Apr 27	0.4	z'	$19' \times 29'$	$0\farcs57$	30	airmass
KAO	2019 May 03	1.3	z'	$12\farcm2 \times 12\farcm2$	$0\farcs357$	40	airmass
KCP	2019 May 03	1.0	z'	$12\farcm2 \times 12\farcm2$	$0\farcs24$	30	airmass

Note. All the follow-up photometry presented in this paper is available in machine-readable form. See Collins et al. (2018) for a detailed description of the KELT-FUN facilities.

Table 3
Relative Out of Transit Radial Velocities for KELT-24 from TRES

BJD_{TDB}	RV (m s^{-1})	σ_{RV} (m s^{-1})	Bisectors	σ_{Bis}
2458548.824216	402.7	20.4	−8.7	64.5
2458566.788751	877.4	38.1	−33.4	60.1
2458568.804163	159.8	22.8	−33.2	72.5
2458569.643873	−27.6	32.9	−86.8	66.0
2458570.638165	151.7	27.7	197.2	77.6
2458570.893951	291.2	24.4	−23.5	56.4
2458571.650562	726.4	29.2	−14.0	45.0
2458571.768010	734.4	25.4	−127.6	60.3
2458572.781102	801.4	58.1	37.8	116.0
2458573.918608	303.8	28.7	89.0	42.4
2458574.618596	130.8	36.5	14.4	63.8
2458575.626432	15.1	24.5	9.8	55.6
2458576.685400	423.3	30.4	9.9	53.6
2458577.655622	820.4	25.7	−95.1	55.8
2458577.812743	860.0	31.6	−56.8	46.7
2458586.716848	−11.2	33.2	100.8	94.4
2458591.721299	39.8	43.2	−199.2	108.3
2458594.763412	914.2	35.9	−112.1	63.8
2458597.690503	−29.5	42.4	−84.6	58.3

Table 4
Median Values and 68% Confidence Interval for Global Model of KELT-24

Parameter	Units	Values
Stellar Parameters:		
M_*	Mass ($M_\odot$)	$1.460^{+0.055}_{-0.059}$
R_*	Radius ($R_\odot$)	1.506 ± 0.022
L_*	Luminosity ($L_\odot$)	$3.67^{+0.16}_{-0.15}$
ρ_*	Density (cgs)	$0.603^{+0.032}_{-0.033}$
log g	Surface gravity (cgs)	$4.247^{+0.019}_{-0.021}$
$T_{\rm eff}$	Effective Temperature (K)	6509^{+50}_{-49}
[Fe/H]	Metallicity (dex)	$0.186^{+0.077}_{-0.076}$
$[Fe/H]_0$[a]	Initial Metallicity	$0.284^{+0.059}_{-0.058}$
Age	Age (Gyr)	$0.78^{+0.61}_{-0.42}$
EEP[b]	Equal Evolutionary Point	323^{+16}_{-23}
$v \sin I_*$	Projected rotational velocity (km s^{-1})	19.76 ± 0.160
ξ	Macroturbulence velocity (km s^{-1})	$5.76^{+0.51}_{-0.50}$

Notes.
[a] The initial metallicity is the metallicity of the star when it was formed.
[b] The Equal Evolutionary Point corresponds to static points in a star's evolutionary history when using the MIST isochrones and can be a proxy for age. See Section 2 in Dotter (2016) for a more detailed description of EEP.

young age of KELT-24 suggests it has just started to evolve from the zero-age main sequence, which is consistent with our UVW analysis (see Section 2.7).

We detected a nonzero, small 3σ eccentricity of $0.077^{+0.024}_{-0.025}$ for KELT-24 b's orbit. However, systems observed to have small eccentricities (<0.1) are subject to the Lucy–Sweeney bias, where observational errors of a circular orbit can lead to the detection of a slight eccentricity (Lucy & Sweeney 1971). Therefore, we caution the reader about the detection of the eccentricity, even though it is detected at a formally significant confidence level. We do note that this eccentricity was not only constrained by the spectroscopic observations from TRES (see Section 2.3) but also from the KELT-FUN transit observations (i.e., the transit duration), because they are all globally modeled with EXOFASTv2 (see Section 3). Because the eccentricity is quite small and not conclusive, we use Equation (3) from Adams & Laughlin (2006) to approximate the circularization timescale of KELT-24 b to be 12.7 Gyr (assuming $Q_\star = 10^6$). This circularization timescale does not change significantly when accounting for the small eccentricity detected. Since the age of KELT-24 is significantly smaller than the circularization timescale, we do not assume the eccentricity to be zero within our global analysis. Future observations should confirm this nonzero eccentricity by obtaining additional higher precision RVs and/or observing the secondary eclipse of KELT-24 b. The time difference between the secondary eclipse assuming zero eccentricity and one using e = 0.078 from our results is about 3.5 hr. Future eclipse observations should account for this when scheduling eclipse observations. KELT-24 has a projected rotational velocity of 19.46 ± 0.18 km s^{-1}, corresponding to a rotation period of 3.9 days. Since this is shorter than the orbital period of KELT-24 b we do not expect the planet to be tidally synchronized.

4.1. Tidal Evolution and Irradiation History

We calculated the past and future orbital evolution of the orbit of KELT-24 b under the influence of tides, using the POET code (Penev et al. 2014). We calculated the evolution of the orbital semimajor axis (see Figure 9) under the assumptions of a constant tidal phase lag (or constant tidal quality factor), circular orbit, and no perturbations due to further, undetected, objects in the system. Under these assumptions, the tides that the star raises on the planet have no appreciable effect on the orbit, because the angular momentum that can be stored/extracted from the planet is a negligible fraction of the total orbital angular momentum. As a result, the tidal evolution is

Table 5
Median Values and 68% Confidence Interval for Global Model of KELT-24

Parameter	Description (Units)	Values		
P	Period (days)	$5.5514926^{+0.0000081}_{-0.0000080}$		
R_P	Radius (R_J)	1.272 ± 0.021		
T_C	Time of conjunction (BJD_{TDB})	$2457147.0529^{+0.0020}_{-0.0021}$		
T_0[a]	Optimal conjunction time (BJD_{TDB})	$2458540.47759^{+0.00036}_{-0.00035}$		
a	Semimajor axis (au)	$0.06969^{+0.00087}_{-0.00096}$		
i	Inclination (deg)	$89.17^{+0.59}_{-0.75}$		
e	Eccentricity	$0.077^{+0.024}_{-0.025}$		
ω_*	Argument of periastron (deg)	55^{+13}_{-15}		
T_{eq}	Equilibrium temperature (K)	1459 ± 16		
M_P	Mass (M_J)	$5.18^{+0.21}_{-0.22}$		
K	RV semi-amplitude (m s^{-1})	462^{+16}_{-15}		
$\log K$	Log of RV semi-amplitude	2.665 ± 0.015		
R_P/R_*	Radius of planet in stellar radii	$0.08677^{+0.00071}_{-0.00070}$		
a/R_*	Semimajor axis in stellar radii	$9.95^{+0.17}_{-0.18}$		
δ	Transit depth (fraction)	0.00753 ± 0.00012		
Depth	Flux decrement at mid transit	0.00753 ± 0.00012		
τ	Ingress/egress transit duration (days)	$0.01458^{+0.00084}_{-0.00029}$		
T_{14}	Total transit duration (days)	$0.17917^{+0.0011}_{-0.00097}$		
T_{FWHM}	FWHM transit duration (days)	$0.16442^{+0.00081}_{-0.00080}$		
b	Transit impact parameter	$0.134^{+0.13}_{-0.096}$		
b_S	Eclipse impact parameter	$0.15^{+0.13}_{-0.11}$		
τ_S	Ingress/egress eclipse duration (days)	$0.01677^{+0.00068}_{-0.00062}$		
$T_{S,14}$	Total eclipse duration (days)	$0.2028^{+0.0096}_{-0.010}$		
$T_{S,FWHM}$	FWHM eclipse duration (days)	$0.1861^{+0.0090}_{-0.0100}$		
$\delta_{S,3.6\ \mu m}$	Blackbody eclipse depth at 3.6 μm (ppm)	431 ± 14		
$\delta_{S,4.5\ \mu m}$	Blackbody eclipse depth at 4.5 μm (ppm)	599 ± 17		
ρ_P	Density (cgs)	3.13 ± 0.19		
$\log g_P$	Surface gravity	$3.900^{+0.021}_{-0.022}$		
λ	Projected spin–orbit alignment (deg)	$2.6^{+5.1}_{-3.6}$		
Θ	Safronov number	0.389 ± 0.014		
$\langle F \rangle$	Incident flux (10^9 erg s^{-1} cm^{-2})	$1.022^{+0.043}_{-0.042}$		
T_P	Time of periastron (BJD_{TDB})	$2457146.60^{+0.17}_{-0.22}$		
T_S	Time of eclipse (BJD_{TDB})	$2457144.423^{+0.060}_{-0.056}$		
T_A	Time of ascending node (BJD_{TDB})	$2457145.842^{+0.053}_{-0.057}$		
T_D	Time of descending node (BJD_{TDB})	2457148.398 ± 0.048		
$e \cos \omega_*$		$0.041^{+0.017}_{-0.016}$		
$e \sin \omega_*$		$0.063^{+0.023}_{-0.027}$		
$M_P \sin i$	Minimum mass (M_J)	$5.18^{+0.21}_{-0.22}$		
M_P/M_*	Mass ratio	$0.00339^{+0.00013}_{-0.00012}$		
d/R_*	Separation at mid transit	9.32 ± 0.39		
P_T	A priori nongrazing transit prob	$0.0980^{+0.0043}_{-0.0040}$		
$P_{T,G}$	Apriori transit prob	$0.1166^{+0.0051}_{-0.0047}$		
P_S	A priori nongrazing eclipse prob	$0.08622^{+0.0020}_{-0.00084}$		
$P_{S,G}$	A priori eclipse prob	$0.1026^{+0.0025}_{-0.0010}$		
Wavelength Parameters:		R	i'	z'
u_1	Linear limb-darkening coeff	0.258 ± 0.046	0.217 ± 0.027	0.148 ± 0.021
u_2	Quadratic limb-darkening coeff	$0.320^{+0.049}_{-0.048}$	0.323 ± 0.028	0.300 ± 0.022
A_D	Dilution from neighboring stars	$0.01004^{+0.00050}_{-0.00051}$	0.01761 ± 0.00088	0.0268 ± 0.0013
Telescope Parameters:		TRES		
γ_{rel}	Relative RV offset (m s^{-1})	416^{+12}_{-11}		
σ_J	RV jitter (m s^{-1})	33^{+16}_{-14}		
σ_J^2	RV jitter variance	1150^{+1300}_{-740}		
Doppler Tomography Parameters:				
σ_{DT}	Doppler tomography Error scaling	0.9932 ± 0.0095	...	...

Notes. See Table 3 in Eastman et al. (2019) for a list of the derived and fitted parameters in EXOFASTv2.
[a] Minimum covariance with period. All values in this table for the secondary occultation of KELT-24 b are predicted values from our global analysis.

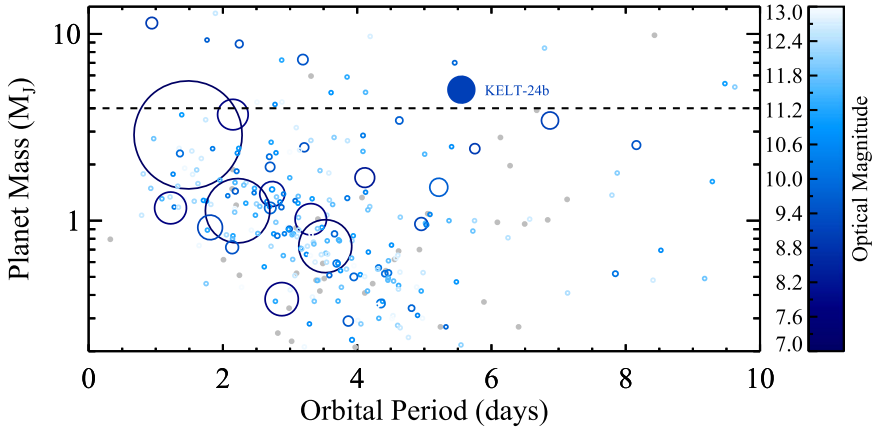

Figure 8. Distribution of planet mass and orbital period for the known population of radial velocity only (gray) and transiting hot Jupiters (colored by optical magnitude). The size of the circle is scaled by the host star's apparent brightness. The filled-in circle represents the location of KELT-24 b. We only show systems that have a 3σ or better measurement on the planet's mass. The horizontal dashed line is the lower limit (4 M_J) of the massive hot Jupiters regime we discuss in Section 4. The data behind this figure was downloaded from the composite table on UT 2019 May 07 from the NASA Exoplanet Archive (Akeson et al. 2013).

Table 6
Median Values and 68% Confidence Interval for Global Model of KELT-24

Transit Parameters		KeplerCam UT 2019 Mar 30 (i')	ULMT UT 2019 Mar 30 (z')	KeplerCam UT 2019 Apr 10 (i')
σ^2	Added variance	$0.00000330^{+0.00000036}_{-0.00000032}$	$0.00000115^{+0.00000017}_{-0.00000015}$	$0.00000834^{+0.0000011}_{-0.00000097}$
F_0	Baseline flux	1.00015 ± 0.00027	1.00017 ± 0.00011	1.00026 ± 0.00058
C_0	Additive detrending coeff	-0.00086 ± 0.00058	$0.00019^{+0.00022}_{-0.00023}$	0.0007 ± 0.0013
C_1	Additive detrending coeff	⋯	0.00032 ± 0.00022	⋯
Transit Parameters:		ULMT UT 2019 Apr 11 (z')	SOTES UT 2019 Apr 16 (R)	CROW UT 2019 Apr 27 (i')
σ^2	Added variance	$0.00000680^{+0.00000085}_{-0.00000073}$	$-0.00000069^{+0.00000049}_{-0.00000040}$	$0.0000370^{+0.0000057}_{-0.0000048}$
F_0	Baseline flux	0.99985 ± 0.00021	$1.00034^{+0.00041}_{-0.00040}$	2.9437 ± 0.0013
C_0	Additive detrending coeff	⋯	-0.00060 ± 0.00077	$0.00451^{+0.00085}_{-0.00084}$
Transit Parameters:		LCO TFN UT 2019 Apr 27 (z')	KAO UT 2019 May 03 (z')	KCP UT 2019 May 03(z')
σ^2	Added variance	$0.0000333^{+0.0000034}_{-0.0000030}$	$0.00000560^{+0.00000054}_{-0.00000048}$	$0.0000260^{+0.0000028}_{-0.0000025}$
F_0	Baseline flux	$1.00556^{+0.00079}_{-0.00077}$	1.00246 ± 0.00029	0.99967 ± 0.00039
C_0	Additive detrending coeff	$-0.0000^{+0.0016}_{-0.0015}$	$0.00266^{+0.00060}_{-0.00059}$	-0.0003 ± 0.0032

dominated by the dissipation of tidal perturbations in the star. We accounted for the evolution of the stellar radius, assuming a MIST (Choi et al. 2016; Dotter 2016) stellar evolutionary track appropriate for the best-fit stellar mass and metallicity from our global fit (see Section 3). Finally, we combined the evolution of the orbital semimajor axis with the evolution of the stellar luminosity per the same MIST model to calculate the evolution of the amount of irradiation received by the planet (see Figure 9). Because the tidal dissipation in stars is poorly constrained, and likely not well described by a simple constant phase lag model, we considered a broad range of plausible phase lags, parameterized by the commonly used tidal dissipation parameter $Q'_\star$ (the ratio of the tidal quality factor $Q_\star$ and the Love number, k2).

Regardless of the tidal quality factor, we concluded that the planet has always been subject to a level of irradiation several times larger than the 2×10^8 erg s^{-1} cm^{-2} threshold Demory & Seager (2011) suggest is required for the planet to be significantly inflated. Also, again regardless of the amount of dissipation, the planet has undergone at most moderate orbital evolution prior to its current, nearly circular orbit. In contrast, the future fate of the planet is significantly impacted by the amount of tidal dissipation assumed. For a tidal quality factor of $Q'_\star = 10^5$, the planet will be engulfed by its parent star within a few hundred Myr, while for $Q'_\star = 10^7$ or larger the planet survives until the end of the main sequence life of its parent star.

4.2. KELT-24's Aligned Orbit

KELT-24 b's aligned orbit is interesting in the context of its mass, possible small eccentricity, and the young age of the system. Hébrard et al. (2010) noted that for massive hot Jupiters, their orbits are typically prograde but with a nonzero misalignment angle, a pattern that still holds true today (see Figure 10). KELT-24 b is therefore somewhat unusual in that its sky-projected spin–orbit misalignment λ is consistent with zero, although the true 3D spin–orbit misalignment ψ could be larger if the host star is not viewed equator-on. We cannot measure the inclination of the stellar rotation axis $I_\star$ using our current data, but a *TESS* measurement of the rotation period via spot modulation or asteroseismology could allow this measurement.

Furthermore, KELT-24's young age and slightly eccentric, aligned orbit place some constraints upon the past history of the system. Some of the high-eccentricity migration mechanisms, such as the Kozai–Lidov mechanism (Anderson et al. 2016) or secular planet–planet interactions (Petrovich & Tremaine 2016)

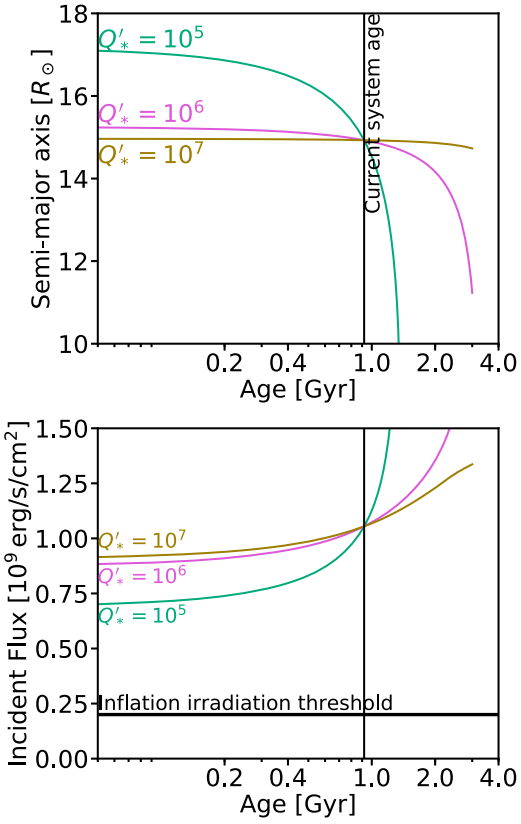

Figure 9. Evolution of the semimajor axis (top) and irradiation (bottom) for KELT-24 b shown for a range of values for $Q^\star$. The color of the line indicates the dissipation in the star (green: $Q_\star = 10^5$, lavender: $Q_\star = 10^7$, gold: $Q_\star = 10^8$).

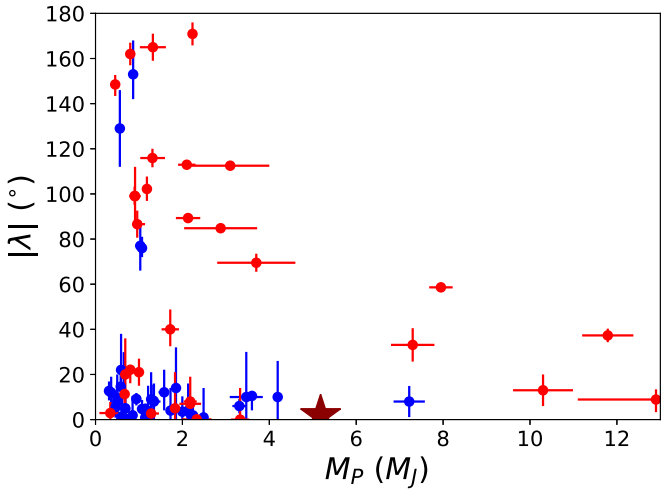

Figure 10. Spin–orbit misalignment of KELT-24b in context with the population of hot Jupiters from the literature. We show the sky-projected spin–orbit misalignments $|\lambda|$ as a function of planetary mass. Red and blue plot points denote planets orbiting stars with effective temperatures less than or greater than the Kraft break at 6250 K, respectively; hot Jupiters orbiting cooler stars typically have well-aligned orbits, whereas those orbiting hotter stars like KELT-24 have a wide range of misalignments (Winn 2010). We highlight KELT-24b as the large dark red star; the uncertainties are smaller than the plot symbol size. We show only planets with measured masses rather than upper limits, and uncertainties on the spin–orbit misalignments of less than 20°.

may take hundreds of Myr and typically leave planets in highly eccentric, misaligned orbits. Together with the long tidal damping timescale for the system (longer than the age of the universe), this suggests that KELT-24 b likely instead migrated through a faster, less dynamically violent mechanism such as interactions with the protoplanetary disk or in situ formation.

4.3. Atmospheric Characterization Prospects

As mentioned, KELT-24 b is one of the few known massive giant planets orbiting a host star bright enough to allow for detailed atmospheric characterization observations. The other comparable planets in this mass range that have been observed with either *Spitzer* or *HST* are HAT-P-2 b (*Spitzer*, Lewis et al. 2014), WASP-14 b (*Spitzer*, Wong et al. 2015), Kepler-13A b (*Spitzer* and *HST*, Beatty et al. 2017), KELT-1b (*Spitzer*, Beatty et al. 2019), and WASP-103b (*Spitzer* and *HST*, Kreidberg et al. 2018). Interestingly, KELT-24 b orbits the brightest host in this regime and has the lowest blackbody equilibrium temperature of all these planets: approximately 1450 K. This places KELT-24 b in a different and potentially interesting atmospheric regime. Given the similarities between HAT-P-2b and KELT-24, future atmospheric observation KELT-24 b would provide a nice comparison to those already taken for HAT-P-2b.

Observations of massive field brown dwarfs have shown that there is a strong blueward shift in the NIR colors of these objects as they cool from roughly 1400 K down to approximately 1000 K. This is known as the "L–T" transition, and is generally believed to represent the clouds in the atmospheres of the hotter L-dwarfs slowly dropping below the level of the photosphere in the cooler T-dwarfs. The few observations we have of giant exoplanets in this regime indicate that this transition may occur at cooler temperatures, presumably because the lower surface gravity of the planets is altering the cloud dynamics in their atmospheres, perhaps allowing vertical lofting to maintain the clouds higher for longer (Triaud et al. 2015).

KELT-24 b possesses an intermediate surface gravity, 3 times higher than Jupiter but 10 times lower than a brown dwarf, that straddles previous observations. The characterization of the global cloud properties on KELT-24 b therefore could allow us to better understand the dynamical processes behind the L–T transition. In particular, a recent analysis of *Spitzer* phase-curve results by Beatty et al. (2019) has shown that all hot Jupiters appear to posses a nightside cloud deck at a temperature of roughly 1000 K. The relatively low equilibrium temperature of KELT-24 b's atmosphere indicates that even dayside clouds on KELT-24 b would be close in composition to the universal nightside clouds on other hot Jupiters. The spectroscopic measurement of KELT-24 b's emission might, therefore, be able to determine the specific composition of these clouds. Cloud compositions would in turn provide invaluable insight into the cloud condensation processes, and hence dynamics.

5. Conclusion

We present the discovery of KELT-24 b, a massive hot Jupiter in a 5.6 day orbit around a young F-star. The host star, HD 93148, is a bright ($V = 8.3$ mag) young F-star ($M_\star = 1.460^{+0.055}_{-0.059}\,M_\odot$, $R_\star = 1.506 \pm 0.022\,R_\odot$, age $= 0.78^{+0.61}_{-0.42}$ Gyr) with a moderate rotation of $v \sin I_* = 19.76 \pm 0.160$ km s^{-1}. The planet is a massive hot Jupiter ($M_P = 5.18^{+0.21}_{-0.22}\,M_J$) on a nearly circular ($e = 0.077^{+0.024}_{-0.025}$) prograde orbit ($\lambda = 2.6^{+5.1}_{-3.6}$ degrees). KELT-24 is the brightest host star with a transiting

massive Jupiter ($M_P > 4\,M_J$), making it well-suited for detailed characterization through eclipse spectroscopy with current facilities like the *HST* and upcoming observatories such as the *James Webb Space Telescope*. KELT-24 b is expected to be observed by NASA's *TESS* mission during sectors 20 and 21, from late UT 2019 December to the end of UT 2020 February. This presents a unique opportunity to simultaneously observe the *TESS* transits of KELT-24 b with *Spitzer*, *HST*, and/or ground-based facilities. Additionally, *TESS* may be able to measure the rotation period of KELT-24, in which case the true (3D) obliquity can be inferred.

We thank Laura Kreidberg, Andrew Vanderburg, and James Kirk for their valuable discussions and insight. J.E.R. was supported by the Harvard Future Faculty Leaders Postdoctoral fellowship. Work by G.Z. is provided by NASA through Hubble Fellowship grant HST-HF2-51402.001-A awarded by the Space Telescope Science Institute, which is operated by the Association of Universities for Research in Astronomy, Inc., for NASA, under contract NAS 5-26555. K.G.S. acknowledges support from the Vanderbilt Office of the Provost through the Vanderbilt Initiative in Data-intensive Astrophysics. T.N and A.Y. are also grateful to Mizuki Isogai, Akira Arai, and Hideyo Kawakita for their technical support on observations at Koyama Astronomical Observatory. This work is partly supported by JSPS KAKENHI grant Numbers JP18H01265 and JP18H05439, and JST PRESTO grant No. JPMJPR1775. J.L.-B. acknowledges support from FAPESP (grant 2017/23731-1). K.P. acknowledges support from NASA grants 80NSSC18K1009 and NNX17AB94G.

This work makes use of observations from the LCOGT network. This research has made use of SAO/NASA's Astrophysics Data System Bibliographic Services. This research has made use of the SIMBAD database, operated at CDS, Strasbourg, France. This work has made use of data from the European Space Agency (ESA) mission *Gaia* (https://www.cosmos.esa.int/gaia), processed by the *Gaia* Data Processing and Analysis Consortium (DPAC, https://www.cosmos.esa.int/web/gaia/dpac/consortium). Funding for the DPAC has been provided by national institutions, in particular, the institutions participating in the *Gaia* Multilateral Agreement. This work makes use of observations from the LCO network. This research has made use of the NASA Exoplanet Archive, which is operated by the California Institute of Technology, under contract with the National Aeronautics and Space Administration under the Exoplanet Exploration Program.

MINERVA is a collaboration among the Harvard-Smithsonian Center for Astrophysics, The Pennsylvania State University, the University of Montana, and the University of Southern Queensland. MINERVA is made possible by generous contributions from its collaborating institutions and Mt. Cuba Astronomical Foundation, The David & Lucile Packard Foundation, National Aeronautics and Space Administration (EPSCOR grant NNX13AM97A), The Australian Research Council (LIEF grant LE140100050), and the National Science Foundation (grants 1516242 and 1608203). Any opinions, findings, and conclusions or recommendations expressed are those of the author and do not necessarily reflect the views of the National Science Foundation. Funding for MINERVA data-analysis software development is provided through a subaward under NASA award MT-13-EPSCoR-0011.

The Center for Exoplanets and Habitable Worlds is supported by the Pennsylvania State University, the Eberly College of Science, and the Pennsylvania Space Grant Consortium.

The ASAS-SN observations are used to help vet exoplanet candidates from KELT. ASAS-SN would like to thank Las Cumbres Observatory and its staff for their continued support. ASAS-SN is funded in part by the Gordon and Betty Moore Foundation through grant GBMF5490 to the Ohio State University, NSF grant AST-1515927, the Mt. Cuba Astronomical Foundation, the Center for Cosmology and Astro-Particle Physics (CCAPP) at OSU, the Chinese Academy of Sciences South America Center for Astronomy (CASSACA), and the Villum Fonden (Denmark).

Facilities: FLWO 1.5 m (Tillinghast Reflector Echelle Spectrograph, TRES); Kilodegree Extremely Little Telescope (KELT); MINiature Exoplanet Radial Velocity Array (MINERVA); Las Cumbres Observatory at Tenerife (LCO TFN); University of Louisville Manner Telescope (ULMT, Mt. Lemmon); KeplerCam (FLWO 1.2m); Stacja Obserwacji Tranzytów Egzoplanet w Suwałkach (SOTES); CROW Observatory; Koyama Astronomical Observatory (KAO).

Software: EXOFASTv2 (Eastman et al. 2013; Eastman 2017), AstroImageJ (Collins et al. 2017), SPC (Buchhave et al. 2010).

ORCID iDs

Joseph E. Rodriguez https://orcid.org/0000-0001-8812-0565
Jason D. Eastman https://orcid.org/0000-0003-3773-5142
George Zhou https://orcid.org/0000-0002-4891-3517
Samuel N. Quinn https://orcid.org/0000-0002-8964-8377
Thomas G. Beatty https://orcid.org/0000-0002-9539-4203
Kaloyan Penev https://orcid.org/0000-0003-4464-1371
Marshall C. Johnson https://orcid.org/0000-0002-5099-8185
David W. Latham https://orcid.org/0000-0001-9911-7388
Allyson Bieryla https://orcid.org/0000-0001-6637-5401
Karen A. Collins https://orcid.org/0000-0001-6588-9574
Courtney D. Dressing https://orcid.org/0000-0001-8189-0233
Fumi Yoshida https://orcid.org/0000-0002-3286-911X
Michael B. Lund https://orcid.org/0000-0003-2527-1598
Daniel J. Stevens https://orcid.org/0000-0002-5951-8328
Keivan G. Stassun https://orcid.org/0000-0002-3481-9052
B. Scott Gaudi https://orcid.org/0000-0003-0395-9869
Knicole D. Colón https://orcid.org/0000-0001-8020-7121
Joshua Pepper https://orcid.org/0000-0002-3827-8417
Norio Narita https://orcid.org/0000-0001-8511-2981
Lehman H. Garrison https://orcid.org/0000-0002-9853-5673
Matthew A. Cornachione https://orcid.org/0000-0003-1012-4771
Jonathan Labadie-Bartz https://orcid.org/0000-0002-2919-6786
Xinyu Yao https://orcid.org/0000-0003-4554-5592
Daniel Bayliss https://orcid.org/0000-0001-6023-1335
Michael L. Calkins https://orcid.org/0000-0002-2830-5661
Jessie L. Christiansen https://orcid.org/0000-0002-8035-4778
Dax Feliz https://orcid.org/0000-0002-2457-7889
Benjamin J. Fulton https://orcid.org/0000-0003-3504-5316

Thomas W.-S. Holoien https://orcid.org/0000-0001-9206-3460
David J. James https://orcid.org/0000-0001-5160-4486
Tharindu Jayasinghe https://orcid.org/0000-0002-6244-477X
Hannah Jang-Condell https://orcid.org/0000-0002-7639-1322
Eric L. N. Jensen https://orcid.org/0000-0002-4625-7333
Somayeh Khakpash https://orcid.org/0000-0002-1910-7065
Mark Manner https://orcid.org/0000-0002-9411-7271
Jennifer L. Marshall https://orcid.org/0000-0003-0710-9474
Kim K. McLeod https://orcid.org/0000-0001-9504-1486
Ryan J. Oelkers https://orcid.org/0000-0002-0582-1751
Matthew T. Penny https://orcid.org/0000-0001-7506-5640
Phillip A. Reed https://orcid.org/0000-0002-5005-1215
B. J. Shappee https://orcid.org/0000-0003-4631-1149
Chris Stockdale https://orcid.org/0000-0003-2163-1437
Thiam-Guan Tan https://orcid.org/0000-0001-5603-6895
Steven Villanueva, Jr. https://orcid.org/0000-0001-6213-8804
Robert A. Wittenmyer https://orcid.org/0000-0001-9957-9304
Jason T. Wright https://orcid.org/0000-0001-6160-5888

References

Adams, F. C., & Laughlin, G. 2006, ApJ, 649, 1004
Akeson, R. L., Chen, X., Ciardi, D., et al. 2013, PASP, 125, 989
Albrecht, S., Winn, J. N., Johnson, J. A., et al. 2012, ApJ, 757, 18
Anderson, K. R., Storch, N. I., & Lai, D. 2016, MNRAS, 456, 3671
Baraffe, I., Chabrier, G., & Barman, T. 2008, A&A, 482, 315
Barclay, T., Pepper, J., & Quintana, E. V. 2018, ApJS, 239, 2
Barnes, S. I., Gibson, S., Nield, K., & Cochrane, D. 2012, Proc. SPIE, 8446, 844688
Batygin, K., Bodenheimer, P. H., & Laughlin, G. P. 2016, ApJ, 829, 114
Beatty, T. G., Madhusudhan, N., Tsiaras, A., et al. 2017, AJ, 154, 158
Beatty, T. G., Marley, M. S., Gaudi, B. S., et al. 2019, AJ, 158, 166
Bensby, T., Feltzing, S., & Lundström, I. 2003, A&A, 410, 527
Bieryla, A., Collins, K., Beatty, T. G., et al. 2015, AJ, 150, 12
Bodenheimer, P., D'Angelo, G., Lissauer, J. J., Fortney, J. J., & Saumon, D. 2013, ApJ, 770, 120
Borucki, W. J., Koch, D., Basri, G., et al. 2010, Sci, 327, 977
Bovy, J. 2017, MNRAS, 470, 1360
Brahm, R., Espinoza, N., Jordán, A., et al. 2019, AJ, 158, 45
Brown, T. M., Baliber, N., Bianco, F. B., et al. 2013, PASP, 125, 1031
Buchhave, L. A., Bakos, G. Á, Hartman, J. D., et al. 2010, ApJ, 720, 1118
Buchhave, L. A., Latham, D. W., Carter, J. A., et al. 2011, ApJS, 197, 3
Buchhave, L. A., Latham, D. W., Johansen, A., et al. 2012, Natur, 486, 375
Cegla, H. M., Lovis, C., Bourrier, V., et al. 2016, A&A, 588, A127
Chabrier, G. 2003, PASP, 115, 763
Chabrier, G., Baraffe, I., Selsis, F., et al. 2007, in Protostars and Planets V, ed. B. Reipurth, D. Jewitt, & K. Keil (Tucson, AZ: Univ. Arizona Press), 623
Chabrier, G., Johansen, A., Janson, M., & Rafikov, R. 2014, in Protostars and Planets VI, ed. H. Beuther et al. (Tucson, AZ: Univ. Arizona Press), 619
Choi, J., Dotter, A., Conroy, C., et al. 2016, ApJ, 823, 102
Ciardi, D. R., Beichman, C. A., Horch, E. P., & Howell, S. B. 2015, ApJ, 805, 16
Coşkunoğlu, B., Ak, S., Bilir, S., et al. 2011, MNRAS, 412, 1237
Collier Cameron, A., Guenther, E., Smalley, B., et al. 2010, MNRAS, 407, 507
Collins, K. A., Collins, K. I., Pepper, J., et al. 2018, AJ, 156, 234
Collins, K. A., Eastman, J. D., Beatty, T. G., et al. 2014, AJ, 147, 39
Collins, K. A., Kielkopf, J. F., Stassun, K. G., & Hessman, F. V. 2017, AJ, 153, 77
Cutri, R. M., Skrutskie, M. F., van Dyk, S., et al. 2003, yCat, 2246, 0
D'Angelo, G., Kley, W., & Henning, T. 2003, ApJ, 586, 540
Dawson, R. I., & Johnson, J. A. 2018, ARA&A, 56, 175
Demory, B.-O., & Seager, S. 2011, ApJS, 197, 12
Dotter, A. 2016, ApJS, 222, 8
Eastman, J. 2017, EXOFASTv2: Generalized Publication-quality Exoplanet Modeling Code, Astrophysics Source Code Library, ascl:1710.003
Eastman, J., Gaudi, B. S., & Agol, E. 2013, PASP, 125, 83
Eastman, J. D., Rodriguez, J. E., Agol, E., et al. 2019, arXiv:1907.09480
Fabrycky, D., & Tremaine, S. 2007, ApJ, 669, 1298
Fűrész, G. 2008, PhD thesis, Univ. Szeged
Furlan, E., Ciardi, D. R., Everett, M. E., et al. 2017, AJ, 153, 71
Gaia Collaboration, Brown, A. G. A., Vallenari, A., et al. 2018, A&A, 616, A1
Gaudi, B. S., Stassun, K. G., Collins, K. A., et al. 2017, Natur, 546, 514
Gaudi, B. S., & Winn, J. N. 2007, ApJ, 655, 550
Gibson, S., Barnes, S. I., Hearnshaw, J., et al. 2012, Proc. SPIE, 8446, 844648
Goldreich, P., & Tremaine, S. 1980, ApJ, 241, 425
Hauschildt, P. H., Allard, F., & Baron, E. 1999, ApJ, 512, 377
Hébrard, G., Désert, J. M., Díaz, R. F., et al. 2010, A&A, 516, A95
Høg, E., Fabricius, C., Makarov, V. V., et al. 2000, A&A, 355, L27
Huang, C., Wu, Y., & Triaud, A. H. M. J. 2016, ApJ, 825, 98
Jayasinghe, T., Kochanek, C. S., Stanek, K. Z., et al. 2018, MNRAS, 477, 3145
Jensen, E. 2013, Tapir: A Web Interface for Transit/eclipse Observability, Astrophysics Source Code Library, ascl:1306.007
Johnson, M. C., Rodriguez, J. E., Zhou, G., et al. 2018, AJ, 155, 100
Kochanek, C. S., Shappee, B. J., Stanek, K. Z., et al. 2017, PASP, 129, 104502
Kovács, G., Bakos, G., & Noyes, R. W. 2005, MNRAS, 356, 557
Bakos, G. Á, Kovács, G., Torres, G., et al. 2007, ApJ, 670, 826
Kreidberg, L., Line, M. R., Parmentier, V., et al. 2018, AJ, 156, 17
Kuhn, R. B., Rodriguez, J. E., Collins, K. A., et al. 2016, MNRAS, 459, 4281
Kurucz, R. L. 1992, in IAU Symp. 149, The Stellar Populations of Galaxies, ed. B. Barbuy & A. Renzini (Dordrecht: Kluwer), 225
Latham, D. W., Mazeh, T., Stefanik, R. P., Mayor, M., & Burki, G. 1989, Natur, 339, 38
Latham, D. W., Stefanik, R. P., Torres, G., et al. 2002, AJ, 124, 1144
Lewis, N. K., Showman, A. P., Fortney, J. J., Knutson, H. A., & Marley, M. S. 2014, ApJ, 795, 150
Lin, D. N. C., Bodenheimer, P., & Richardson, D. C. 1996, Natur, 380, 606
Lucy, L. B., & Sweeney, M. A. 1971, AJ, 76, 544
Lund, M. B., Rodriguez, J. E., Zhou, G., et al. 2017, AJ, 154, 194
Lutz, T. E., & Kelker, D. H. 1973, PASP, 85, 573
Mayor, M., & Queloz, D. 1995, Natur, 378, 355
McLaughlin, D. B. 1924, ApJ, 60, 22
McLeod, K. K., Rodriguez, J. E., Oelkers, R. J., et al. 2017, AJ, 153, 263
Mollière, P., & Mordasini, C. 2012, A&A, 547, A105
Nagasawa, M., & Ida, S. 2011, ApJ, 742, 72
Nidever, D. L., Marcy, G. W., Butler, R. P., Fischer, D. A., & Vogt, S. S. 2002, ApJS, 141, 503
Nielsen, L. D., Bouchy, F., Turner, O., et al. 2019, A&A, 623, A100
Nordstroem, B., Latham, D. W., Morse, J. A., et al. 1994, A&A, 287, 338
Paxton, B., Bildsten, L., Dotter, A., et al. 2011, ApJS, 192, 3
Paxton, B., Cantiello, M., Arras, P., et al. 2013, ApJS, 208, 4
Paxton, B., Marchant, P., Schwab, J., et al. 2015, ApJS, 220, 15
Penev, K., Zhang, M., & Jackson, B. 2014, PASP, 126, 553
Pepper, J., Kuhn, R. B., Siverd, R., James, D., & Stassun, K. 2012, PASP, 124, 230
Pepper, J., Pogge, R. W., DePoy, D. L., et al. 2007, PASP, 119, 923
Pepper, J., Siverd, R. J., Beatty, T. G., et al. 2013, ApJ, 773, 64
Pepper, J., Stassun, K. G., & Gaudi, B. S. 2018, in Handbook of Exoplanets, ed. H. J. Deeg & J. A. Belmonte (Cham: Springer), 128
Petrovich, C., & Tremaine, S. 2016, ApJ, 829, 132
Quinn, S. N., White, R. J., Latham, D. W., et al. 2012, ApJL, 756, L33
Rasio, F. A., & Ford, E. B. 1996, Sci, 274, 954
Ricker, G. R., Winn, J. N., Vanderspek, R., et al. 2015, JATIS, 1, 014003
Rodriguez, J. E., Quinn, S. N., Huang, C. X., et al. 2019, AJ, 157, 191
Rossiter, R. A. 1924, ApJ, 60, 15
Schlegel, D. J., Finkbeiner, D. P., & Davis, M. 1998, ApJ, 500, 525
Shappee, B. J., Prieto, J. L., Grupe, D., et al. 2014, ApJ, 788, 48
Shporer, A., Wong, I., Huang, C. X., et al. 2019, AJ, 157, 178
Siverd, R. J., Beatty, T. G., Pepper, J., et al. 2012, ApJ, 761, 123
Siverd, R. J., Collins, K. A., Zhou, G., et al. 2018, AJ, 155, 35
Spiegel, D. S., Burrows, A., & Milsom, J. A. 2011, ApJ, 727, 57
Stassun, K. G., & Torres, G. 2018, ApJ, 862, 61
Stevens, D. J., Collins, K. A., Gaudi, B. S., et al. 2017, AJ, 153, 178
Swift, J. J., Bottom, M., Johnson, J. A., et al. 2015, JATIS, 1, 027002
Temple, L. Y., Hellier, C., Albrow, M. D., et al. 2017, MNRAS, 471, 2743
Torres, G., Bakos, G. Á, Kovács, G., et al. 2007, ApJL, 666, L121
Triaud, A. H. M. J., Gillon, M., Ehrenreich, D., et al. 2015, MNRAS, 450, 2279
Villanueva, S., Jr., Dragomir, D., & Gaudi, B. S. 2019, AJ, 157, 84

Wilson, M. L., Eastman, J. D., Cornachione, M. A., et al. 2019, PASP, 131, 115001
Winn, J. N. 2010, in Exoplanets, ed. S. Seager (Tucson, AZ: Univ. Arizona Press), 55
Winn, J. N., Fabrycky, D., Albrecht, S., & Johnson, J. A. 2010, ApJL, 718, L145
Wong, I., Knutson, H. A., Lewis, N. K., et al. 2015, ApJ, 811, 122
Wu, Y., & Lithwick, Y. 2011, ApJ, 735, 109
Wu, Y., & Murray, N. 2003, ApJ, 589, 605
Yao, X., Pepper, J., Gaudi, B. S., et al. 2019, AJ, 157, 37
Zacharias, N., Finch, C., & Frouard, J. 2017, yCat, 1340, 0
Zhou, G., Latham, D. W., Bieryla, A., et al. 2016a, MNRAS, 460, 3376
Zhou, G., Rodriguez, J. E., Collins, K. A., et al. 2016b, AJ, 152, 136
Zhou, G., Rodriguez, J. E., Vanderburg, A., et al. 2018, AJ, 156, 93